

PV-OSIMr: A Lowest Order Complexity Algorithm for Computing the Delassus Matrix

Ajay Suresha Sathya¹, Wilm Decré² and Jan Swevers²

Abstract—We present PV-OSIMr, an efficient algorithm for computing the Delassus matrix (also known as the inverse operational space inertia matrix) for a kinematic tree, with the lowest order computational complexity known in literature. PV-OSIMr is derived by optimizing the recently proposed PV-OSIM algorithm using the compositionality of the force and motion propagators. It has a computational complexity of $O(n + m^2)$ compared to $O(n + m^2d)$ of the PV-OSIM algorithm and $O(n + md + m^2)$ of the extended force propagator algorithm (EFPA), where n is the number of joints, m is the number of constraints and d is the depth of the kinematic tree. Since the Delassus matrix is an $m \times m$ sized matrix and its computation must consider all the n joints, PV-OSIMr’s asymptotic computational complexity is optimal. We further benchmark our algorithm and find it to be often more efficient than the PV-OSIM and EFPA in practice.

I. INTRODUCTION

The Delassus matrix [1], also known as the inverse operational space inertia matrix (OSIM), represents the inertial coupling between different constraints on a system of rigid bodies. It is a fundamental physical quantity with applications in robotics and computer graphics such as simulating constrained dynamics [2], [3], simulating contact dynamics [4], [5], [6], operational space control [7], computing the dynamically consistent pseudo-inverse [7], [8] as well as solving inverse dynamics of floating-base robots [9]. The Delassus matrix is named after Etienne Delassus [10] who “first studied the unilateral contact problem with multiple constraints” [1]. The Delassus matrix and inverse OSIM terms have different origins in constrained dynamics [1] and operational space control (where constraints are virtual) literature respectively [7]. These terms refer to the apparent inertia in a given space (whether operational space or constraint space), and are therefore mathematically identical. In this paper, where the main concern is algorithms to compute this quantity, we will use the terms Delassus matrix and inverse OSIM interchangeably.

Computing the Delassus matrix naively from its mathematical definition [7] through dense factorization of the joint space inertia matrix (JSIM) has a high computational complexity of $O(n^3 + m^2n)$, where n is the degrees-of-freedom (DoF) of the mechanism in generalized coordinates and m is the constraint dimension. Considering the centrality of the Delassus matrix in

TABLE I: Computational complexity of various algorithms for inverse OSIM computation.

Algorithm	Complexity
Naive	$O(n^3 + m^2n)$
LTL-OSIM [12]	$O(nd^2 + m^2d + md^2)$
KJR [13]	$O(n + m^2d)$
EFPA [14]	$O(n + md + m^2)$
PV-OSIM [11]	$O(n + m^2d)$
PV-OSIMr (this paper)	$O(n + m^2)$

computationally demanding applications like model predictive control (MPC) and reinforcement learning (RL), where it is often the most expensive step [11] of dynamics computation, an efficient Delassus algorithm is highly desirable and there exists a long tradition of research in this direction.

The Kreutz-Jain-Rodriguez (KJR) algorithm [13] represented a major advance by proposing an $O(n + m^2d)$ complexity recursive Delassus algorithm, where d is the kinematic tree’s depth. This algorithm was further improved in [15] by re-using certain computations to obtain $O(n + mn + m^2)$ complexity. By exploiting extended force propagators (EFP), the EFP algorithm (EFPA) [14] significantly speeds up computing the off-diagonal block of the Delassus matrix, and has the lowest known computational complexity of $O(n + md + m^2)$ in literature. Compared to the complex recursive algorithms mentioned above, [12] presents the simpler LTL-OSIM algorithm that improves upon the naive method by exploiting the branching-induced sparsity in both the JSIM and the constraint Jacobian. Despite its worse complexity of $O(nd^2 + m^2d + md^2)$, the LTL-OSIM algorithm was found [12] to be significantly faster than KJR and competitive with EFPA [14], [11] even for the ASIMO robot (a high DoF humanoid robot with favorable branching structure). Recently, the LTL-OSIM was extended to support kinematic closed loops in [3], which also provided an efficient C++ implementation in the PINOCCHIO library [16].

In our recent work [11], we showed that an existing constrained dynamics algorithm due to Popov and Vereshchagin (PV) [17], [18] computed the Delassus matrix as an intermediate quantity, thereby providing another Delassus algorithm that we called PV-OSIM. The PV-OSIM algorithm has an efficient computation structure requiring only two sweeps compared to three sweeps required by KJR and EFPA. Though PV-OSIM has a higher complexity of $O(n + m^2d)$ compared to EFPA’s $O(n + md + m^2)$ complexity, it was found [11] to be significantly more efficient than the KJR, EFPA and LTL-OSIM for a wide range of robots such as quadrupeds (Go1)

The authors gratefully acknowledge funding from Research Foundation Flanders (FWO) (Grant agreement No. G0D1119N) and Flanders Make SBO project ARENA.

¹ Inria - Département d’Informatique de l’École normale supérieure, PSL Research University. ² Division of Robotics, Automation and Mechatronics in the Department of Mechanical Engineering, KU Leuven, and FlandersMake@KULeuven, Leuven, Belgium ajay.sathya@inria.fr, wilm.decre@kuleuven.be, jan.swevers@kuleuven.be

and humanoids (Atlas and Talos).

However, because of its lower complexity, EFPA scales better than PV-OSIM for long mechanisms with many constraints that need to be propagated through most of the tree's depth. Then the m^2d term in PV-OSIM loses out EFPA's md term. This letter explores whether the PV-OSIM's efficiency can be retained for smaller robots while still scaling better than EFPA to higher DoF robots with many constraints.

A. Approach and contributions

By using the compositionality of EFP, we optimize the PV-OSIM algorithm [11] to propose a new $O(n+m^2)$ complexity Delassus algorithm called PV-OSIMr. This is the lowest order algorithm that we are aware of in the literature (see Table I). Presenting this algorithm and computationally benchmarking it is the main contribution of this paper.

PV-OSIMr (also EFPA and PV-OSIM) however assumes that the constraints are imposed on individual links and would require non-trivial modification for constraints involving multiple links, e.g. a constraint on the center-of-mass (CoM). Supporting such a constraint is relatively easier for the joint-space algorithms like LTL-OSIM [12].

Organization: We introduce the preliminaries and kinematic tree notation in the rest of this section. Then we review LTL-OSIM, extended propagators, PV-OSIM and EFPA in Section II before presenting the PV-OSIMr algorithm in Section III. Identical notation used for all the three recursive algorithms (PV-OSIM, EFPA and PV-OSIMr) facilitates comparing them. Finally, we present numerical benchmarking results in Section IV and conclude in Section V.

B. Preliminaries

Constrained dynamics involves solving the equations

$$M(\mathbf{q})\dot{\boldsymbol{\nu}} + \mathbf{c}(\mathbf{q}, \boldsymbol{\nu}) + J(\mathbf{q})^T \boldsymbol{\lambda} = \boldsymbol{\tau}, \quad (1a)$$

$$J(\mathbf{q})\dot{\boldsymbol{\nu}} + \dot{J}(\mathbf{q}, \boldsymbol{\nu})\boldsymbol{\nu} = \mathbf{k}(\mathbf{q}, \boldsymbol{\nu}), \quad (1b)$$

where $M(\mathbf{q}) \in \mathbb{R}^{n \times n}$ is the symmetric positive definite JSIM, $\mathbf{c}(\mathbf{q}, \boldsymbol{\nu}) \in \mathbb{R}^n$ includes the Coriolis, centrifugal and gravitational force terms, $\boldsymbol{\tau} \in \mathbb{R}^n$ is joint torques, $J(\mathbf{q}) \in \mathbb{R}^{m \times n}$ is the constraint Jacobian matrix, $\boldsymbol{\lambda} \in \mathbb{R}^m$ is Lagrange multipliers denoting the constraint force magnitude, $\mathbf{k} \in \mathbb{R}^m$ is the desired constraint acceleration and $\dot{J}(\mathbf{q}, \boldsymbol{\nu}) \in \mathbb{R}^{m \times n}$ is $J(\mathbf{q})$'s time-derivative. The functional dependence of the expressions will be dropped for brevity from now on.

Solving for $\dot{\boldsymbol{\nu}}$ in Eq. (1a) and substituting in Eq. (1b) gives

$$\Lambda^{-1} \boldsymbol{\lambda} = \dot{J}\boldsymbol{\nu} - \mathbf{k} + JM^{-1}(\boldsymbol{\tau} - \mathbf{c}), \quad (2)$$

where $\Lambda(\mathbf{q})^{-1} := JM^{-1}J^T$ is the Delassus matrix, which maps constraint force magnitudes to constraint accelerations and captures the inertial coupling between constraints.

While the equations above were described in the joint-space, they can also be equivalently described at the link level in 'maximal' coordinates. We use the standard Featherstone's spatial algebra [2] to refer to a rigid-body's physical quantities. Let $\mathbf{a}_i \in \mathbb{M}^6$ and $H_i \in \mathbb{I}^6$ represent the spatial acceleration and spatial inertia of the i th link respectively. S_i is the i th joint's

motion subspace matrix of size $6 \times n_i$, with each column in \mathbb{M}^6 , where n_i the i th joint's DoF. The constraint on a link i can be expressed as

$$K_i(\mathbf{q})\mathbf{a}_i = \mathbf{k}_i(\mathbf{q}, \boldsymbol{\nu}), \quad (3)$$

where $K_i(\mathbf{q}) \in \mathbb{R}^{m_i \times 6}$ is the i th link's constraint matrix and $\mathbf{k}_i(\mathbf{q}, \boldsymbol{\nu}) \in \mathbb{R}^{m_i}$ is the desired i th link's constraint acceleration vector. For more information on spatial algebra and for solving constrained dynamics expressed at the link level, readers are referred to [2] and [11] respectively.

C. Kinematic tree notation

Let all the links of a kinematic tree with n_b bodies be indexed from 1 to n_b , with $i < j$ if the i th link is an ancestor of the j th link in the tree. The i th link's parent joint is also indexed with the number i . The inertial world frame is indexed to be the 0th link. For floating-base trees, the 1st joint, connecting the 0th and 1st links, is a free-flyer joint that permits motion in all 6 directions. Let $\pi(i)$ index the i th link's parent link and $\gamma(i)$ is the set of all the i th link's children links' indices. Let m_b denote the number of motion constraints. To facilitate future notation, we adopt the clever approach from [14] and introduce a fictitious child link for each constraint. This fictitious link is assumed to be rigidly attached to the parent constrained link with coinciding frames. Let these fictitious links, which we call end-effectors, be indexed as $\mathcal{E} = \{n_b + 1, n_b + 2, \dots, n_b + m_b\}$.

Let $\mathcal{S} = \{1, 2, \dots, n_b\}$ be an ordered set and \mathcal{S}_r its reverse. Let $\text{anc}(i)$ and $\text{desc}(i)$ be the set of all link indices that are ancestors and descendants of the i th link in the tree respectively. Let $\text{ES}(i) = \{j \in \mathcal{E} | j \in \text{desc}(i)\}$, be the set indexing all end-effectors supported by the i th link. Let $\text{cca}(i, j) = \mathbf{max}((\text{anc}(i) \cup \{i\}) \cap (\text{anc}(j) \cup \{j\}))$, define the closest common ancestor of the i th and j th links. Let $\mathcal{N} = \{0\} \cup \mathcal{E} \cup \{i \in \mathcal{S} | \text{ES}(j) \subset \text{ES}(i), \forall j \in \gamma(i)\}$, define a set of 'branching links'. Let $\mathcal{A}(i) = \mathbf{max}(\text{anc}(i) \cap \mathcal{N})$ index the closest ancestor branching link, and likewise let $\mathcal{D}(i) = \mathbf{min}((\text{desc}(i) \cup \{i\}) \cap \mathcal{N})$ index the closest descendant branching link. Let $\text{path}(i, j)$ be the set of all joints between i th and j th links.

We will illustrate the terms introduced above using a 6-link tree shown in Fig. 1. Three of its links are constrained, to represent which, three fictitious end-effectors $\mathcal{E} = \{7, 8, 9\}$ are introduced (indicated by green nodes). For this tree, $\mathcal{S} = \{1, 2, 3, 4, 5, 6\}$, $\text{anc}(8) = \{0, 1, 2, 3\}$. As examples of ES, $\text{ES}(5) = \{9\}$, $\text{ES}(3) = \{8, 9\}$ and $\text{ES}(2) = \{7, 8, 9\}$. $\text{cca}(8, 9) = 3$ and $\text{cca}(7, 9) = 2$. The branching links are $\mathcal{N} = \{0, 2, 3, 7, 8, 9\}$. The branching link ancestors and descendants of each link are as follows

$$\begin{bmatrix} i \\ \mathcal{D}(i) \\ \mathcal{A}(i) \end{bmatrix} : \begin{bmatrix} 1 & 2 & 3 & 4 & 5 & 6 & 7 & 8 & 9 \\ 2 & 2 & 3 & 9 & 9 & 7 & 7 & 8 & 9 \\ 0 & 0 & 2 & 3 & 3 & 2 & 2 & 3 & 3 \end{bmatrix}.$$

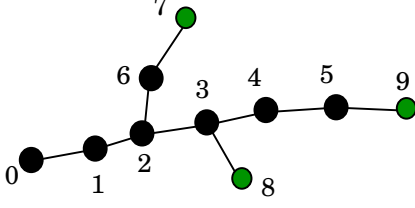


Fig. 1: Schematic diagram of a kinematic tree, nodes are the links, edges are the joints. The green nodes are the fictitious links representing end-effectors.

II. BACKGROUND

We now introduce the LTL-OSIM, PV-OSIM and EFPA algorithms and relevant physical quantities along the way. All the spatial motion vectors, force vectors and inertia matrices are expressed in and with respect to a fixed inertial frame to make the algorithm presentation less cluttered.

A. LTL-OSIM algorithm

The LTL-OSIM algorithm [12] is the simplest among the existing efficient OSIM algorithms. It exploits the branching-induced sparsity in M and J matrices. Let

$$L^T L = M, \quad (4)$$

be the LTL Cholesky decomposition of the JSIM M , where L is a lower triangular matrix. Note that the LTL decomposition above differs from the traditional LLT Cholesky decomposition. LTL preserves M 's sparsity pattern in L [19] when joints are numbers from root to leaves. Let

$$Y = J L^{-1}, \quad (5)$$

where Y shares J 's sparsity pattern. The inverse OSIM Λ^{-1} is given by

$$\Lambda^{-1} = Y Y^T. \quad (6)$$

Despite Λ^{-1} being a dense matrix in general, exploiting sparsity in M , L , J and Y matrices makes LTL-OSIM efficient and competitive with lower complexity algorithms for kinematic trees up to a certain size.

B. Extended propagators

We now review the force and motion propagators used later in this paper. Let H_i^A denote the articulated body inertia (ABI) matrix [20], which is the apparent inertia felt at the i th link considering the subtree rooted at the i th link with all its descendant joints being free to move. Projecting the ABI onto the i th joint's motion subspace yields

$$D_i := S_i^T H_i^A S_i, \quad (7)$$

which is the i th link's apparent inertia felt at the i th joint. Let

$$\pi^{(i)} P_i := (I_{6 \times 6} - H_i^A S_i (D_i)^{-1} S_i^T), \quad (8)$$

denote the projection matrix, that that transmits spatial forces acting on the i th link to its parent link after removing the

force component that causes the i th joint's motion. Trivially, ${}^i P_i := I_{6 \times 6}$. For any end-effector link $i \in \mathcal{E}$, $\pi^{(i)} P_i := I_{6 \times 6}$ since the virtual end-effector link is assumed to be rigidly attached to its parent link.

It is long known [21] that $\pi^{(i)} P_i$'s transpose $\pi^{(i)} P_i^T$ (also a projection matrix) is the motion propagator, that transmits accelerations acting on the parent link $\pi(i)$ to the child link i through the i th joint. The force propagators can be composed [15] to define extended force propagators (EFP)

$${}^j P_i := {}^j P_{\pi(i)} \dots \pi^{(\pi(i))} P_{\pi(i)} \pi^{(i)} P_i, \quad (9)$$

that directly transmit spatial forces backward from the i th link to an ancestral link $j \in \text{anc}(i)$. Analogously, ${}^j P_i^T$ is the extended motion propagator (EMP) that transmits spatial accelerations forward from the j th link to the i th link. Let

$$\pi^{(i)} \Omega_i := S_i (D_i)^{-1} S_i^T, \quad (10)$$

where $\pi^{(i)} \Omega_i \in \mathbb{R}^{6 \times 6}$ denotes the i th link's apparent spatial inverse inertia if the $\pi(i)$ is grounded. Analogously to the EFPs, we now denote ${}^j \Omega_i$ as the i th link's apparent spatial inverse inertia when an ancestral link $j \in \text{anc}(i)$ is grounded, computing which requires accumulating contributions to the i th link's acceleration due to the motion of all joints in $k \in \text{path}(j, i)$ caused by the force acting on the i th link. Each such joint k 's contribution is obtained by back propagating the i th link's force to the k th link using EFP, multiplying it with $\pi^{(k)} \Omega_k$ to compute the resulting k th link's acceleration and forward propagating this acceleration term to the i th link using EMP. Adding these terms gives

$${}^j \Omega_i := \sum_{k \in \text{path}(j, i)} {}^k P_i^T \pi^{(k)} \Omega_k {}^k P_i. \quad (11)$$

To facilitate Delassus matrix computation, which is the constraint space inverse inertia, we now introduce constraint space force and motion propagators. Let

$${}^j K_i := K_i {}^j P_i^T, \quad (12)$$

where, ${}^j K_i$ is the constraint space EMP (CEMP) that forward propagates the j th link's spatial acceleration to the i th link's (an end-effector) constraint space accelerations. Analogously, ${}^j K_i^T$ is the constraint space EFP (CEFP), which back propagates the i th end-effector's constraint force magnitudes (λ_i) to the j th link's spatial forces. Let

$${}^k \Lambda_{i,j}^{-1} := {}^{\text{cca}(i,j)} K_i {}^k \Omega_{\text{cca}(i,j)} {}^{\text{cca}(i,j)} K_j^T, \quad (13)$$

where ${}^k \Lambda_{i,j}^{-1} \in \mathbb{R}^{m_i \times m_j}$, denotes the cross-coupling constraint space inverse inertia mapping λ_j to the i th link's spatial acceleration, if a link $k \in \text{anc}(\text{cca}(i, j))$ is grounded.

We now introduce notation used by PV-OSIM that aggregates terms related to all end-effectors in $\text{ES}(i)$. Let $K_i^A = [\dots {}^i K_j^T \dots]^T$, for $j \in \text{ES}(i)$. Similarly, let

$$L_i^A := \begin{bmatrix} \cdot & \cdot & \cdot \\ \cdot & {}^i \Lambda_{j,k}^{-1} & \cdot \\ \cdot & \cdot & \cdot \end{bmatrix} \quad (14)$$

aggregate all the constraint space inverse inertias for all end-effectors $j, k \in \text{ES}(i)$ for a mechanism grounded at the i th link, with its matrix blocks being the ${}^i\Lambda_{j,k}^{-1}$ terms. Considering the whole tree (where only the ground inertial link 0 is grounded) gives the Delassus matrix

$$\Lambda^{-1} = L_0^A. \quad (15)$$

C. PV-OSIM algorithm

Algorithm 1 lists the PV-OSIM [11] algorithm for completeness. The main computational bottleneck of PV-OSIM is the line 14 which requires $O(m^2d)$ number of operations, while line 13 requires $O(md)$ operations, because computing lines 14 and 13 for all links at a given depth k from the root requires at most $O(m^2)$ and $O(m)$ operations respectively. All the other lines of the algorithm require $O(n)$ or $O(m)$ number of operations, bringing the total complexity to $O(n + m^2d)$.

Algorithm 1 The PV-OSIM algorithm

Require: q , K_i s, robot model

First forward sweep

- 1: **for** i in \mathcal{S} **do**
- 2: $H_i^A \leftarrow H_i$; $K_i^A \leftarrow [\]$; $L_i^A \leftarrow [\]$;

Backward sweep

- 3: **for** i in \mathcal{E}_r **do**
 - 4: $K_{\pi(i)}^A \leftarrow \begin{bmatrix} K_{\pi(i)}^A \\ K_i^A \end{bmatrix}$
 - 5: $L_{\pi(i)}^A \leftarrow \begin{bmatrix} L_{\pi(i)}^A \\ 0_{m_i \times m_i} \end{bmatrix}$
 - 6: **for** i in \mathcal{S}_r **do**
 - 7: $D_i = S_i^T H_i^A S_i$; $\pi(i)\Omega_i = S_i D_i^{-1} S_i^T$
 - 8: **if** $\pi(i) > 0$ **then**
 - 9: $\pi(i)P_i = I_{6 \times 6} - H_i^A \pi(i)\Omega_i$
 - 10: $H_{\pi(i)}^A \leftarrow H_{\pi(i)}^A + \pi(i)P_i H_i^A$
 - 11: **if** $\text{ES}(i) \neq \emptyset$ **then**
 - 12: **if** $\pi(i) > 0$ **then**
 - 13: $K_{\pi(i)}^A \leftarrow \begin{bmatrix} K_{\pi(i)}^A \\ K_i^A \pi(i)P_i^T \end{bmatrix}$
 - 14: $L_{\pi(i)}^A \leftarrow \begin{bmatrix} L_{\pi(i)}^A \\ L_i^A + K_i^A \pi(i)\Omega_i K_i^{AT} \end{bmatrix}$
 - 15: $\Lambda^{-1} = L_0^A$
-

D. Extended force propagator algorithm (EFPA)

Algorithm 2 presents the EFPA. While the recursive CEMP computation in EFPA in line 11 appears different from PV-OSIM's line 13, these two lines are computationally identical. Only the EFPA maintains each end-effector's CEMP separately instead of concatenating them to enable efficient Delassus matrix assembly later. The main difference between PV-OSIM and EFPA arises in line 15, where EFPA recursively computes the term $({}^0\Omega_i^i K_j^T) \in \mathbb{R}^{6 \times m_j}$, which maps each j th end-effector's constraint force magnitudes λ_j to the i th link's spatial acceleration for all ancestors $i \in \text{anc}(j)$. This requires $O(md)$ operations. Then $\frac{m_b(m_b-1)}{2}$ number of ${}^0\Lambda_{i,j}^{-1}$ blocks are computed in line 19 using EFP, bringing EFPA's

total computational complexity to $O(n + md + m^2)$, because $m \propto m_b$.

Algorithm 2 The EFPA algorithm

Require: q , K_i s, robot model

First forward sweep

- 1: **for** i in \mathcal{S} **do**
- 2: $H_i^A \leftarrow H_i$;

Backward sweep

- 3: **for** i in \mathcal{E}_r **do**
- 4: $\pi(i)K_i \leftarrow K_i$
- 5: **for** i in \mathcal{S}_r **do**
- 6: $D_i = S_i^T H_i^A S_i$; $\pi(i)\Omega_i = S_i D_i^{-1} S_i^T$
- 7: **if** $\pi(i) > 0$ **then**
- 8: $\pi(i)P_i = I_{6 \times 6} - H_i^A S_i (D_i)^{-1} S_i^T$
- 9: $H_{\pi(i)}^A \leftarrow H_{\pi(i)}^A + \pi(i)P_i H_i^A$
- 10: **for** $j \in \text{ES}(i)$ **do**
- 11: $\pi(i)K_j = {}^iK_j \pi(i)P_i^T$
- 12: **for** $i \in \mathcal{S}$ **do**
- 13: **for** $j \in \text{ES}(i)$ **do**
- 14: **if** $\pi(i) \neq 0$ **then**
- 15: $({}^0\Omega_i^i K_j^T) = \pi(i)P_i^T ({}^0\Omega_{\pi(i)} \pi(i)K_j^T) + \pi(i)\Omega_i^i K_j^T$
- 16: **else**
- 17: $({}^0\Omega_i^i K_j^T) = {}^0\Omega_i^i K_j^T$

Assembling the Delassus matrix

- 18: **for** $i, j \in \mathcal{E}$, **if** $i \leq j$ **do**
 - 19: ${}^0\Lambda_{i,j}^{-1} = cca(i,j)K_i ({}^0\Omega_{cca(i,j)} cca(i,j)K_j^T)$
-

III. PV-OSIMR ALGORITHM

Equipped with the previous section's notation, we now adapt the PV-OSIM algorithm to obtain the PV-OSIMr algorithm. We first describe the insight that reduces PV-OSIM's complexity and follow that with the PV-OSIMr algorithm.

Insight behind the reduced complexity: The lines 13 and 14 of Algorithm 1 are evaluated over all end-effector supporting links wastefully leading to $O(md)$ and $O(m^2d)$ operations respectively. However, from the line 19 from Algorithm 2, we see that we need to compute iK_j for end-effectors j only at select ancestral branching links i ($i \in \mathcal{N} \cap \text{anc}(j)$), and likewise we need inverse inertias ${}^0\Omega_i$ only at the same select branching links i .

To compute these terms efficiently, we first recursively compute the EFPs and spatial inverse inertia between only the branching links in a backward sweep over all the links $k \in \mathcal{S}_r$ in $O(n)$ operations, as shown in Fig. 2a using

$$\pi^{(k)}\Omega_{\mathcal{D}(k)} = {}^k\Omega_{\mathcal{D}(k)} + {}^kP_{\mathcal{D}(k)}^T S_k (D_k^{-1}) S_k^T {}^kP_{\mathcal{D}(k)}, \quad (16)$$

$$\pi^{(k)}P_{\mathcal{D}(k)} = \pi^{(k)}P_k {}^kP_{\mathcal{D}(k)}. \quad (17)$$

Then in a limited forward sweep over branching links $i \in \mathcal{N}$ as shown in Fig. 2b, the ${}^0\Omega_i$ terms are computed using

$${}^0\Omega_i = \mathcal{A}^{(i)}\Omega_i + \mathcal{A}^{(i)}P_i^T {}^0\Omega_{\mathcal{A}^{(i)}} \mathcal{A}^{(i)}P_i, \quad (18)$$

in $O(n)$ operations. Then for each end-effector j , the CEMPs ${}^i K_j$ are computed from ancestral branching links $i \in (\mathcal{N} - \{0\}) \cap \text{anc}(j)$ recursively in a backward sweep over branching links as shown in Fig. 2c using

$${}^{\mathcal{A}(i)} K_j = {}^i K_j {}^{\mathcal{A}(i)} P_i^T, \quad (19)$$

in at most $O(m^2)$ operations, because the number of branching links (excluding end-effectors and the root link) cannot exceed the number of end-effectors. Finally, Λ^{-1} is assembled by calling Eq. (13) m_b^2 times to compute each of its blocks (${}^0 \Lambda_{i,j}^{-1}$) in $O(m^2)$ as shown in Fig. 2d. This brings the total complexity of PV-OSIMr to $O(n + m^2)$ operations.

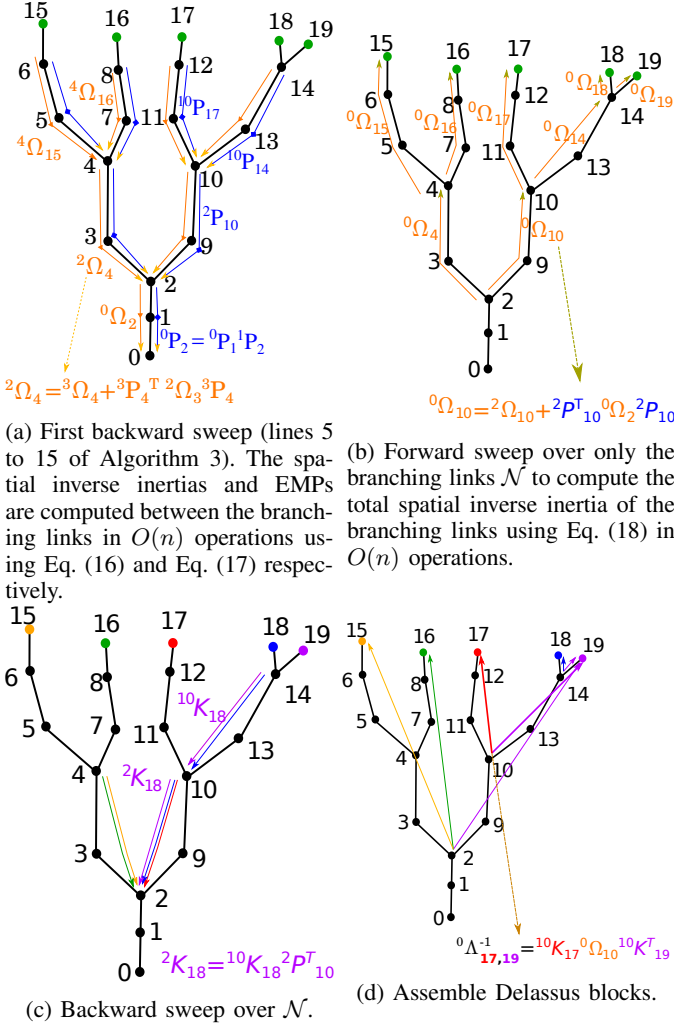


Fig. 2: Graphical illustration of the different computation sweeps in Algorithm 3.

The PV-OSIMr algorithm is presented in Algorithm 3. The algorithm is slightly optimized in line 4 with an abuse of notation by assigning the CEMP to EMP at the end-effector links. This avoids the unnecessary computation of EMP between an end-effector and its ancestral branching link. Furthermore, CEMP and constraint-space inverse inertias are directly available at the end-effectors in lines 20 and 28

respectively, thereby avoiding computations for transforming EMPs and spatial inverse inertias to the constraint space.

Algorithm 3 The PV-OSIMr algorithm

Require: \mathbf{q} , K_i s, robot model

First forward sweep

- 1: **for** i in \mathcal{S} **do**
- 2: $H_i^A \leftarrow H_i$;
- 3: **for** $i \in \mathcal{E}$ **do**
- 4: ${}^{\pi(i)} P_i \leftarrow K_i^T$; ${}^{\pi(i)} \Omega_i \leftarrow 0_{m_i \times m_i}$

Backward sweep

- 5: **for** i in \mathcal{S}_r **do**
- 6: **if** $i \in \mathcal{N}$ **then**
- 7: ${}^i P_i = I_{6 \times 6}$; ${}^i \Omega_i \leftarrow 0_{6 \times 6}$
- 8: $D_i = S_i^T H_i^A S_i$; ${}^{\pi(i)} \Omega_i = S_i D_i^{-1} S_i^T$
- 9: **if** $\pi(i) > 0$ **then**
- 10: ${}^{\pi(i)} P_i = I_{6 \times 6} - H_i^A {}^{\pi(i)} \Omega_i$
- 11: $H_{\pi(i)}^A \leftarrow H_{\pi(i)}^A + {}^{\pi(i)} P_i H_i^A$
- 12: **if** $\text{ES}(i) \neq \emptyset$ **then**
- 13: ${}^{\pi(i)} P_{\mathcal{D}(i)} = {}^{\pi(i)} P_i {}^i P_{\mathcal{D}(i)}$
- 14: **if** $\text{ES}(i) \neq \emptyset$ **then**
- 15: ${}^{\pi(i)} \Omega_{\mathcal{D}(i)} = {}^i \Omega_{\mathcal{D}(i)} + {}^i P_{\mathcal{D}(i)}^T {}^{\pi(i)} \Omega_i {}^i P_{\mathcal{D}(i)}$

Forward sweep over \mathcal{N}

- 16: **for** i in $\mathcal{N} - \{0\}$ **if** $\mathcal{A}(i) \neq 0$ **do**
- 17: ${}^0 \Omega_i = \mathcal{A}(i) \Omega_i + \mathcal{A}(i) P_i^T {}^0 \Omega_{\mathcal{A}(i)} \mathcal{A}(i) P_i$

Backward sweep over \mathcal{N}

- 18: **for** $i \in \mathcal{E}$ **do**
- 19: **if** $\mathcal{A}(i) \neq 0$ **then**
- 20: ${}^{\mathcal{A}(i)} K_i = \mathcal{A}(i) P_i^T$
- 21: **for** j in $(\mathcal{N}_r - \{0\})$ **if** $j \in \text{anc}(i)$, $\mathcal{A}(j) \neq 0$, **do**
- 22: ${}^{\mathcal{A}(j)} K_i = {}^j K_i \mathcal{A}(j) P_j^T$

Assemble the Delassus matrix

- 23: **for** $i, j \in \mathcal{E}$, $i \leq j$ **do**
- 24: **if** $i < j$ **then**
- 25: ${}^0 \Lambda_{i,j}^{-1} = \text{cca}(i,j) K_i {}^0 \Omega_{\text{cca}(i,j)} \text{cca}(i,j) K_j^T$
- 26: ${}^0 \Lambda_{j,i}^{-1} = {}^0 \Lambda_{i,j}^{-T}$
- 27: **else**
- 28: ${}^0 \Lambda_{i,i}^{-1} \leftarrow {}^0 \Omega_i$

IV. RESULTS AND DISCUSSIONS

A. Implementation

Similarly to [11], we have implemented the PV-OSIMr algorithm using the CASADI [22] library. Apart from enabling efficient C code generation for the dynamics algorithms, CASADI implementation enables us to count the number of operations in a given algorithm. We will use this operation count to benchmark PV-OSIMr with our implementation of PV-OSIM, EFPA and LTL-OSIM algorithms. The algorithms presented in this paper assumed that all the quantities are expressed in an inertial frame to avoid the clutter due to spatial transforms. However, the OSIM algorithms (as well as the ABA algorithm [2], [23]) are more efficiently implemented in the local frame. Therefore, our CASADI implementation

is also in the local frame. Readers are referred to the source code¹ of the implementation for further details on the local frame implementation. Note that a C++ implementation of PV-OSIMr is also made available in the PINOCCHIO library [16] and can be found in the `computePvDelassusMatrix()` function of the `delassus.hxx` file². However, the C++ implementation represents physical quantities in inertial frame instead of the more efficient local frame, and improving its efficiency by switching to local frames will be our future work.

B. Computational scaling study

We now analyze the computational scaling of the recursive Delassus algorithms (PV-OSIM, EFPA and PV-OSIMr) w.r.t. increasing tree depth, number of branches and constraints. Consider a mechanism (see Fig. 3a) with a long stem and branches on either side, with each branch consisting of 7 links. Each branch tip is rigidly constrained with a `weld` constraint (6D constraint). This mechanism is chosen because it is a simple mechanism with the property that path lengths, along which the computation sweep over, increases linearly with the stem length for any choice of floating base link. The operation count of the different algorithms for mechanisms with different number of branches is plotted in Fig. 3, with the x-axis denoting the stem length.

When there is only one branch, the mechanism is a serial chain with 6D constraints on each end, and there is no difference between the PV-OSIMr and PV-OSIM algorithms as the dimensionality of the propagated constraints does not exceed 6 to benefit from PV-OSIMr’s optimization w.r.t to PV-OSIM. For two or more branches, PV-OSIMr’s advantage becomes apparent as it scales significantly better than PV-OSIM due to its lower computational complexity. EFPA is more expensive than both PV-OSIMr and PV-OSIM for nearly all the considered mechanisms. As discussed extensively in [11], despite having a lower asymptotic complexity than PV-OSIM, EFPA is more expensive for small mechanisms with few constraints (~ 50) because it has a three sweep structure compared to the two sweep structure of PV-OSIM, and it computes inverse inertia in each link’s frame (see line 15 in Algorithm 2) which requires an expensive similarity transformation during the second forward sweep. However, for long enough mechanisms with sufficiently many constraints the EFPA eventually becomes faster than the PV-OSIM (see Fig. 3f) due to its lower computational complexity.

Scaling when the md term dominates:

While the examples considered above showcase PV-OSIMr’s efficiency, they do not empirically demonstrate its lower complexity. Therefore, we now consider mechanisms where the md term dominates. Consider a serial chain with $n_b = k^2$ bodies and let the links $\{k, 2k \dots k^2\}$ be constrained with 6D constraints. For this mechanism, $n = k^2$, $d = k^2$ and $m = 6k$, $md = 6k^3$ and $m^2 = 36k^2$. Therefore the md term dominates as k increases and PV-OSIMr (with $O(n + m^2)$)

scales as $O(k^2)$, EFPA (with $O(n + md + m^2)$) scales as $O(k^3)$, and PV-OSIM(with $O(n + m^2d)$) scales as $O(k^4)$. The number of operations required by different algorithms for increasing values of k is plotted in a log-log plot in Fig. 4a. PV-OSIMr clearly has the same slope as the $O(k^2)$ function while EFPA has a higher slope due to the md term.

Scaling when $m \propto d$:

We now study the undesirable scenario for PV-OSIMr, when all the links are in \mathcal{N} . Consider a chain with a 6D constraint on all its links. In this case ($n = d = \frac{m}{6}$), both EFPA and PV-OSIMr have the same asymptotic complexity and scale quadratically with n , while PV-OSIMr scales cubically. The results for different algorithms for a chain of increasing sizes is plotted in a log-log plot in Fig. 4b. PV-OSIMr and EFPA are found to have the same slope as expected. However, PV-OSIMr remains significantly faster than EFPA even in this example, mainly because of the way EFPA propagates a separate inverse inertia term for every supported end-effector (see line 15 in Algorithm 2) requiring $O(md)$ operations. In contrast, PV-OSIMr computes all inverse inertia terms in only $O(n)$ operations.

C. Humanoid robot standing constraints

We now compare the different OSIM algorithms (PV-OSIMr, PV-OSIM, EFPA and LTL) for a humanoid robot Atlas and the results are tabulated in Fig. 5. The number of operations required to compute the inverse OSIM when the Atlas robot is standing, which is modeled as each of its feet being rigidly connected to the world with a 6D `weld` constraint is plotted in Fig. 5a. The hip link to which both the legs are connected is selected as the floating base. There is no difference between PV-OSIM and PV-OSIMr in this case as the two 6D constraints meet only at the floating-base link during the backward propagation and therefore does not benefit from the PV-OSIMr’s improvement.

Next, we consider the example where the foot-ground constraint is modelled as `connect`-type 3D constraints at four contact points as is commonly done to model foot contact wrench cone [24]. PV-OSIM propagates 12D constraints from each foot while PV-OSIMr only propagates 6D constraints leading to a reduction in computation cost with PV-OSIM requiring 19.9% more operations than PV-OSIMr. For both examples, the PV-OSIM and PV-OSIMr significantly outperform EFPA and LTL.

D. Humanoid robot with shadow hands

Finally, we compare the OSIM algorithms for an Atlas robot equipped with the Shadow hand in Fig. 6. We impose a 3D `connect` type constraint on each fingertip of the hand leading to a total of 15D constraints. We plot the OSIM results for i) just a single Shadow hand, ii) an Atlas robot with a single shadow hand connected to its left wrist, iii) an Atlas robot with a shadow hand connected to each wrist, and iv) finally an Atlas robot with both its feet constrained with 6D `weld` constraints on each foot in addition to the 15D constraint on

¹https://github.com/AjSat/spatial_V2

²<https://github.com/stack-of-tasks/pinocchio/blob/master/include/pinocchio/algorithm/recursive/pv-osimr.cpp>

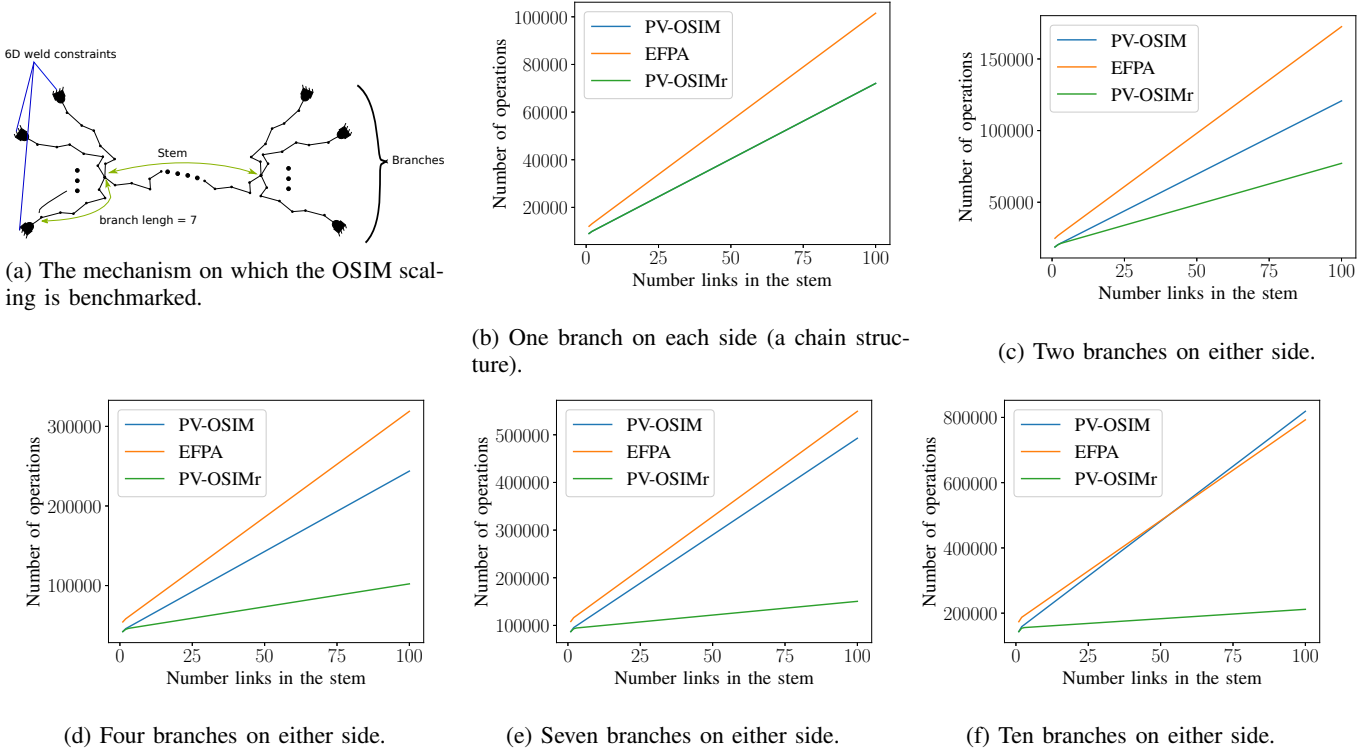


Fig. 3: Benchmarking the number of operations of the different OSIM algorithms.

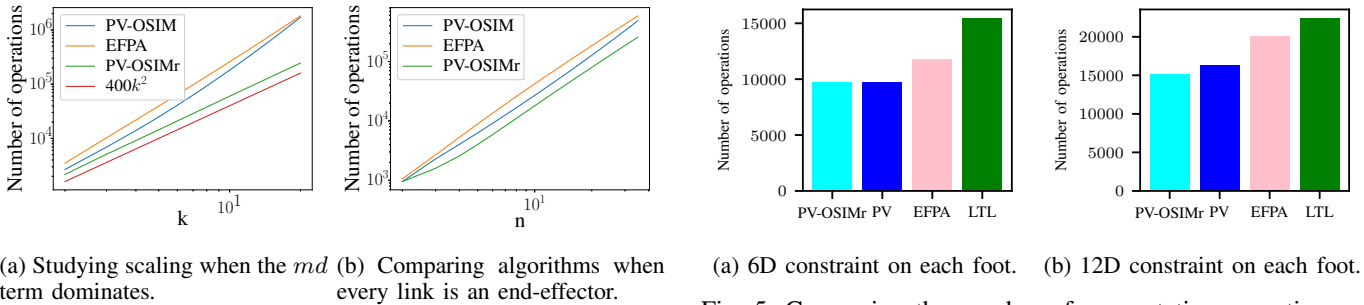


Fig. 4: Comparing the scaling of the recursive algorithms on more mechanisms.

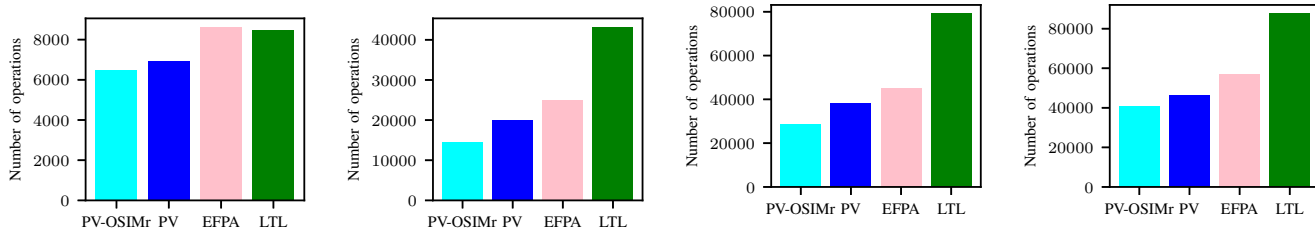
Fig. 5: Comparing the number of computation operations of the OSIM algorithms for the Atlas robot.

each shadow hand in Fig. 6a, Fig. 6b, Fig. 6c and Fig. 6d respectively.

The typically expensive LTL-OSIM is computationally more efficient than EFPA for just the Shadow Hand in Fig. 6a because the LTL-OSIM benefits from the sparsity induced by the extensive branching of the hand’s mechanism. When the Shadow hand is connected to the Atlas robot in the remaining three examples, the performance of the high complexity LTL-OSIM significantly deteriorates compared to the lower complexity algorithms PV-OSIMr, PV-OSIM and EFPA. The PV-OSIMr algorithm is found to be significantly more efficient than the other algorithms with up to $\sim 34\%$ fewer operations needed than the next most efficient algorithm PV-OSIM.

E. Caveats

While PV-OSIMr outperforms PV-OSIM in all the examples presented so far, we note that there were some cases when PV-OSIM was more efficient. This occurs especially when more than six constraints need to be propagated in PV-OSIM through only a few (≤ 3) single DoF joints, because for single DoF joints PV-OSIM recursively computes the OSIM through efficient symmetric rank-1 (SR1) updates per joint (by computing the vector $K_i^A S_i$, see line 14 in Algorithm 1). PV-OSIMr instead performs two symmetric rank-6 computations (see line 25 and line 17 in Algorithm 3), which are more expensive than SR1 updates over a few joints. For example, if a 6D weld constraint is imposed on both the hands (without the Shadow Hand) in addition to the 6D constraints on the feet



(a) Considering a single shadow hand, a 24 d.o.f system. Connect Atlas's left wrist with same constraint (3D) on each fingertip strain as in Fig. 6a (total 15 constraints leading to 15 constraints).
 (b) Shadow hand connected to Atlas's left wrist with same constraints on a 60 d.o.f system).

(c) Shadow hand connected to both wrists of Atlas with each strained as in Fig. 6c along with hand having the same constraints (6D weld constraint on each foot as in Fig. 6a (total 30 constraints for standing. total 42 constraints on an 84 d.o.f system)).
 (d) Atlas with both hands connected with each strained as in Fig. 6c along with hand having the same constraints (6D weld constraint on each foot as in Fig. 6a (total 30 constraints for standing. total 42 constraints on an 84 d.o.f system)).

Fig. 6: Comparing the number of computation operations of the OSIM algorithms for the Atlas robot equipped with the shadow hand.

of Atlas considered in Section IV-C, the PV-OSIM requires $\sim 1.5\%$ fewer operations than PV-OSIMr, because PV-OSIM's simpler backward pass remains more efficient when performed over just three joints (from sternum to the floating base hip link).

V. CONCLUSIONS

We presented PV-OSIMr, an algorithm with the lowest known computational complexity of $O(n + m^2)$ to compute the Delassus matrix or the inverse OSIM matrix, which is a fundamental quantity with various simulation and control applications in a computationally demanding setting. Our algorithm is conceived by re-ordering and eliminating unnecessary computations from the PV-OSIM algorithm. The PV-OSIMr algorithm not only has the lowest computational complexity, but is also found to lead to up to 24% improvement over practical examples involving the Atlas robot. Furthermore, since computing the inverse OSIM matrix requires considering all the n joints and populating a dense matrix of size $m \times m$, the achieved computational complexity of $O(n + m^2)$ can be considered asymptotically optimal.

REFERENCES

- [1] B. Brogliato, *Nonsmooth Mechanics: Models, Dynamics and Control*. Springer, 2016.
- [2] R. Featherstone, *Rigid body dynamics algorithms*. Springer, 2014.
- [3] J. Carpentier, R. Budhiraja, and N. Mansard, "Proximal and sparse resolution of constrained dynamic equations," in *Proc. Robot., Sci. Syst.*, 2021.
- [4] C. Duriez, F. Dubois, A. Kheddar, and C. Andriot, "Realistic haptic rendering of interacting deformable objects in virtual environments," *IEEE Trans. Vis. Comput. Graph.*, vol. 12, no. 1, pp. 36–47, 2005.
- [5] M. L. Felis, "Rbdl: an efficient rigid-body dynamics library using recursive algorithms," *Autonomous Robots*, vol. 41, no. 2, pp. 495–511, 2017.
- [6] J. Hwangbo, J. Lee, and M. Hutter, "Per-contact iteration method for solving contact dynamics," *IEEE Robot. Autom. Lett.*, vol. 3, no. 2, pp. 895–902, 2018. [Online]. Available: www.raism.com
- [7] O. Khatib, "A unified approach for motion and force control of robot manipulators: The operational-space formulation," *IEEE Journal on Robotics and Automation*, vol. 3, no. 1, pp. 43–53, 1987.
- [8] A. Dietrich, C. Ott, and A. Albu-Schäffer, "An overview of null space projections for redundant, torque-controlled robots," *Int. J. Robot. Res.*, vol. 34, no. 11, pp. 1385–1400, 2015.
- [9] L. Righetti, J. Buchli, M. Mistry, M. Kalakrishnan, and S. Schaal, "Optimal distribution of contact forces with inverse-dynamics control," *Int. J. Robot. Res.*, vol. 32, no. 3, pp. 280–298, 2013.
- [10] É. Delassus, "Mémoire sur la théorie des liaisons finies unilatérales," in *Annales scientifiques de l'École normale supérieure*, vol. 34, 1917, pp. 95–179.
- [11] A. S. Sathya, H. Bruyninckx, W. Decré, and G. Pipeleers, "Efficient constrained dynamics algorithms based on an equivalent lqr formulation using gauss' principle of least constraint," *IEEE Trans. Robot.*, vol. 40, pp. 729–749, 2024.
- [12] R. Featherstone, "Exploiting sparsity in operational-space dynamics," *Int. J. Robot. Res.*, vol. 29, no. 10, pp. 1353–1368, 2010.
- [13] K. Kreuz-Delgado, A. Jain, and G. Rodriguez, "Recursive formulation of operational-space control," *Int. J. Robot. Res.*, vol. 11, no. 4, pp. 320–328, 1992.
- [14] P. Wensing, R. Featherstone, and D. E. Orin, "A reduced-order recursive algorithm for the computation of the operational-space inertia matrix," in *Proc. IEEE Int. Conf. Robot. Autom.* IEEE, 2012, pp. 4911–4917.
- [15] K.-S. Chang and O. Khatib, "Efficient recursive algorithm for the operational space inertia matrix of branching mechanisms," *Advanced Robotics*, vol. 14, no. 8, pp. 703–715, 2001.
- [16] J. Carpentier, G. Saurel, G. Buondonno, J. Mirabel, F. Lamiraux, O. Stasse, and N. Mansard, "The pinocchio c++ library: A fast and flexible implementation of rigid body dynamics algorithms and their analytical derivatives," in *2019 IEEE/SICE International Symposium on System Integration (SII)*. IEEE, 2019, pp. 614–619.
- [17] J. P. Popov, A. F. Vereshchagin, and S. L. Zenkevič, *Manipulacionnyje roboty: Dinamika i algoritmy*. Nauka, 1978.
- [18] A. F. Vereshchagin, "Modeling and control of motion of manipulative robots," *Soviet Journal of Computer and Systems Sciences*, vol. 27, no. 5, pp. 29–38, 1989.
- [19] R. Featherstone, "Efficient factorization of the joint-space inertia matrix for branched kinematic trees," *Int. J. Robot. Res.*, vol. 24, no. 6, pp. 487–500, 2005.
- [20] —, "The calculation of robot dynamics using articulated-body inertias," *Int. J. Robot. Res.*, vol. 2, no. 1, pp. 13–30, 1983.
- [21] K. W. Lilly, "Efficient dynamic simulation of multiple chain robotic systems," Ph.D. dissertation, Dept. of Electrical Engineering, The Ohio State University, 1989.
- [22] J. A. Andersson, J. Gillis, G. Horn, J. B. Rawlings, and M. Diehl, "Casadi: a software framework for nonlinear optimization and optimal control," *Mathematical Programming Computation*, vol. 11, no. 1, pp. 1–36, 2019.
- [23] M. Otter, H. Brandl, and R. Johanni, "An algorithm for the simulation of multibody systems with kinematic loops," in *Proceedings of the 7th World Congress on Theory of Machines and Mechanisms, IFToMM, Sevilla, Spain*, 1987.
- [24] S. Caron, Q.-C. Pham, and Y. Nakamura, "Stability of surface contacts for humanoid robots: Closed-form formulae of the contact wrench cone for rectangular support areas," in *Proc. IEEE Int. Conf. Robot. Autom.* IEEE, 2015, pp. 5107–5112.